Inorganic Chemistry

pubs.acs.org/IC

Featured Article

# Modulating Structural and Electronic Properties of Rare Archimedean and Johnson-Type Mn Cages

Swetanshu Tandon, Friedrich W. Steuber, Amal C. Kathalikkattil, Munuswamy Venkatesan, Graeme W. Watson,* and Wolfgang Schmitt*

Cite This: *Inorg. Chem.* 2021, 60, 8388−8393

Read Online

ACCESS | Metrics & More | Article Recommendations | Supporting Information

**ABSTRACT:** High-nuclearity Mn complexes have attracted significant scientific attention due to their fascinating magnetic properties and their relevance to bioinorganic systems and catalysis. In this work, we demonstrate how the strong binding characteristics of phosphonate ligands can be coupled with sterically hindered carboxylate groups to influence the symmetry of Mn coordination clusters. We describe the structure of two high-nuclearity Mn coordination cages, $\{Mn_{12}\}$ and $\{Mn_{15}\}$, synthesized using this approach. These cages are structurally related to the truncated tetrahedral geometry and adopt rare topological features of Archimedean and Johnson-type solids. Their structural attributes distinctively influence their magnetic properties and electrocatalytic $H_2O$ oxidation characteristics.

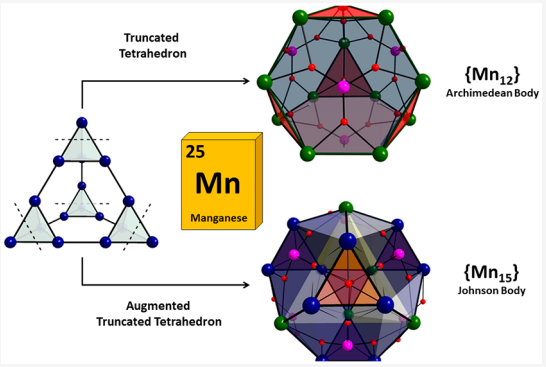


## INTRODUCTION

High-nuclearity oxo/hydroxo-clusters represent a fascinating subclass of supramolecular compounds.[1−3] The symmetry, connectivity of the metal centers, and the resulting topological features of these systems affect not only their electronic properties but also the chemical activity.[4−8] Hence, synthetic ligand- or metal-directed assembly approaches may provide pathways to such molecule-based materials with desirable and tunable properties. High nuclearity Mn clusters have captured significant attention in the last few decades.[2,9−16] Their key characteristics stem from the presence of unpaired electrons and Jahn−Teller distortions which, in combination with intriguing structural features, can give rise to unusual magnetic properties, including slow relaxation of the magnetization,[2] colossal magnetoresistance,[9] or magnetocaloric effects.[17−19] Additionally, Mn-based coordination clusters are of relevance to bioinorganic chemistry[20−23] and catalysis.[24−28] Relevant polynuclear compounds have been extensively investigated particularly in relation to the oxygen evolution reaction (OER)[29−35] primarily due to nature's use of a tetranuclear Mn species to catalyze this highly endergonic reaction.[21,22,25,36,37]

The synthesis of polynuclear Mn species often relies on self-assembly approaches which are serendipitous by nature.[38] Ligand choice, however, imparts some synthetic control that influences the binding affinity toward metal ions, sterics, denticity, and the bridging behavior.

We have previously exploited the high binding affinity and defined bridging capabilities of phosphonate ligands to synthesize high nuclearity V and Mn based Archimedean[39] and Platonic bodies, and Keplerates.[40−42] Here, we demonstrate the possibility of combining the binding attributes of phosphonate ligands with those of sterically hindered carboxylates to modulate the symmetry of Mn coordination clusters whose core structures are based on unusual truncated tetrahedral topologies.

We report rare examples of Archimedean[39] ($[Mn^{II}_{12}(\mu_3\text{−}OH)_4(PhPO_3)_4(^tBuCO_2)_{12}(DMSO)_6]$, (**1**), and Johnson[43] ($[Mn^{II}_5Mn^{III}_{10}(\mu_3\text{-}O)_4(^tBuCO_2)_{7.15}(MeCO_2)_{4.85}(PhPO_3)_6(\mu\text{-}OMe)_6(\mu_3\text{-}OMe)_2(MeOH)_5]$, (**2**), type solids. The synthesis, structure, and magnetic characterization of these clusters are reported. Importantly, we demonstrate how the symmetry of the core structure of these clusters influences the electrocatalytic properties toward the highly endergonic, proton-coupled water oxidation reaction in neutral aqueous media.

## RESULTS AND DISCUSSION

Single crystals of **1** were obtained by reacting $KMnO_4$ and Mn(II) acetate in a MeCN/DMSO mixture in the presence of sterically demanding pivalate and strongly binding phenylphosphonate ligands. It should be noted that a relative excess of pivalic acid is required to suppress the formation of

**Received:** March 30, 2021
**Published:** June 2, 2021

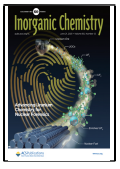









https://doi.org/10.1021/acs.inorgchem.1c00984
*Inorg. Chem.* 2021, 60, 8388−8393

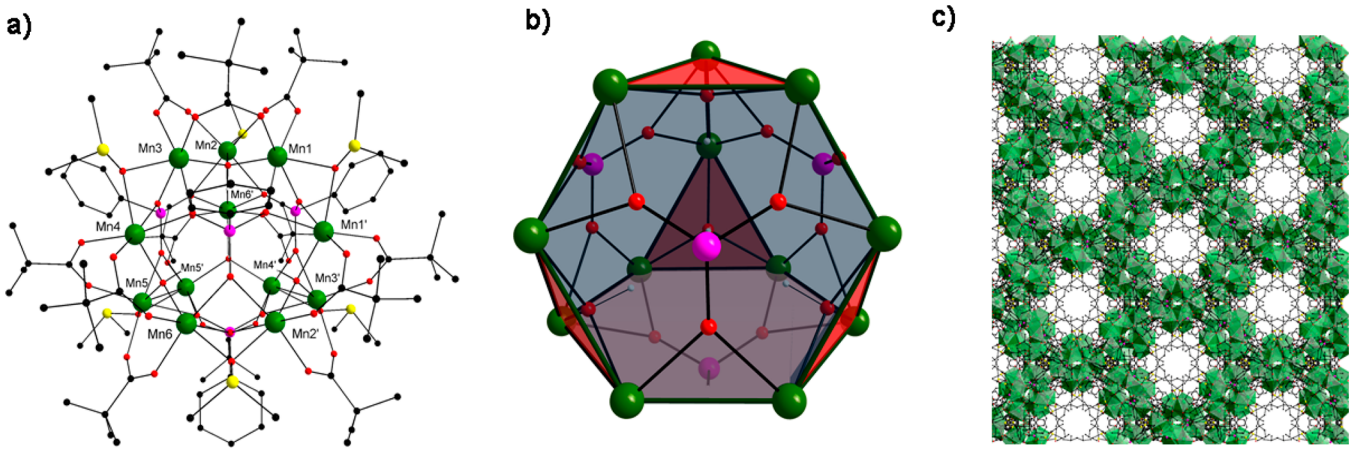


**Figure 1.** (a) Crystal structure of **1**, (b) core structure of the complex highlighting the truncated tetrahedral geometry, (c) packing diagram in polyhedral representation of **1** with view in the direction of the crystallographic *c*-axis. Color scheme: Mn (green), S (yellow), P (pink), C (black), O (red). H atoms omitted for clarity; symmetry key '= +Y, + X, 3/2-Z.

phosphonate salts illustrating the strong binding ability of the phosphonate ligands. The solvent mixture also plays an important role in the synthesis as it facilitates the solubility of both ligand types. Solvent variations, i.e., replacement of DMSO with DMF preferentially results in the formation of a well-known $\{Mn_6\}$ cluster.[44] L(−)-proline assists the crystallization process of **1** and may act as a structure influencing agent[41] or a "silent ligand".[45−47] Importantly, it tends to stabilize the +II oxidation state of the Mn centers in compound **1** as the absence of L(−)-proline in the reaction mixture was found to lead to a dark solution characteristic of the formation of Mn species that stabilize +III oxidation states (see also compound **2**).

The structure of **1** (Figure 1a) was solved and refined in the rhombohedral space group $R\bar{3}c$, with half the cluster entity located in the asymmetric unit. The dodecanuclear coordination compound **1** adopts a highly symmetric core structure representing an unusual example of a truncated tetrahedral Archimedean body and resembles the rare $\varepsilon$-Keggin structure[48] in which the central tetrahedral ion is removed. The $Mn^{II}$ centers reside at the vertices of a truncated tetrahedron and adopt octahedral coordination environments (Figure 1b). The $Mn^{II}$ ions of the four triangular faces assemble around central $\mu_3$-$OH^-$ groups and are capped by three syn, syn-bidentate pivalate ligands. The $\mu_3$-$OH^-$ ligands are located below the mean plane of the three $Mn^{II}$ centers (∼0.37 Å) toward the center of the coordination cage. The hexagonal faces involving six $Mn^{II}$ centers are capped by phenylphosphonate ligands which bind in characteristic 6.222 modes.[49] Bridging $\mu_2$-$\kappa$O−DMSO molecules complete the molecular entity. Bond valence sum (BVS) analysis[50,51] confirm the +II oxidation states of all Mn atoms and the nature of the bridging $OH^-$ groups. The packing of the coordination clusters **1** in the crystal structure is stabilized by weak dispersion forces between the organic ligand residues. These forces result in a typical honeycomb-type assembly whereby the screw axes coincide with the centers of the resulting hexagons (Figure 1c).

Among transition metal clusters, the truncated tetrahedral geometry is only rarely observed[52−54] whereby only one Mn coordination cluster with highly distorted truncated tetrahedral geometry has been reported.[55] To determine the extent of distortion from an ideal truncated tetrahedron of the cage in **1**, continuous shape measure analysis[56,57] was performed as implemented in SHAPE.[58] This analysis (SI) gives a value of 0.139 indicating negligible distortions from the ideal geometry and making **1** the first example of a highly regular Archimedean truncated tetrahedral Mn cluster.

A second, structurally related, unprecedented cluster with lower symmetry is formed when the synthetic procedure of **1** is modified. A reaction of $KMnO_4$, Mn(II) acetate, pivalic acid, and phenylphosphonic acid in a MeCN/MeOH mixture in the presence of 2,6-pyridinedimethanol and acetic acid yields a highly asymmetric pentadecanuclear cluster, **2**. The crystal structure solution and refinement for **2** were achieved in the rhombohedral space group *R*3 with the whole cluster entity located in the asymmetric unit.

Mn centers in **2** adopt octahedral coordination environments and occupy the vertices of a distorted augmented truncated tetrahedron which has, additionally, a triangular cupola unit attached to one of the hexagonal faces (Figure 2). To our best knowledge, **2** serves as the only example that forms this characteristic Johnson-type geometrical arrangement. As highlighted in Figure 2a, the Mn4−Mn15 centers reside at the vertices of the distorted truncated tetrahedron while Mn1−Mn3 provide the additional vertices. In contrast to **1**, the phenylphosphonate groups cap hexagonal and pentagonal faces binding in 6.222 and 5.221 modes, respectively (see Figure 3 for comparison to binding mode in **1**). **2** can further be conceptualized as a congregation of triangular $\{Mn_3\}$ units which are bridged by *syn*, *syn*-bidentate carboxylate functionalities of pivalates and acetates. These $\{Mn_3\}$ units form around central $\mu_3$-$O^{2-}$ oxo-groups and are stabilized by coordinating MeOH ligands. Differently, the triangular unit comprising Mn1−Mn3 is centered around two $\mu_3$-$OMe^-$ groups of which one resides in the cage while the other is located outside. BVS analysis[50,51] confirms the mixed-valent nature of the compound which is composed of 5 $Mn^{II}$ and 10 $Mn^{III}$. The coordination environments of the latter display characteristic Jahn−Teller distortions, which are in-line with the lower symmetry of **2** in comparison to **1**. The lower symmetry also translates to the packing of coordination clusters of **2** in the crystal structure. Here, dispersion forces between the residues of the ligands result in triangular-shaped voids that extend in the direction of the crystallographic *c*-axis which contain constitutional solvent molecules (Figure S5).


https://doi.org/10.1021/acs.inorgchem.1c00984
Inorg. Chem. 2021, 60, 8388−8393

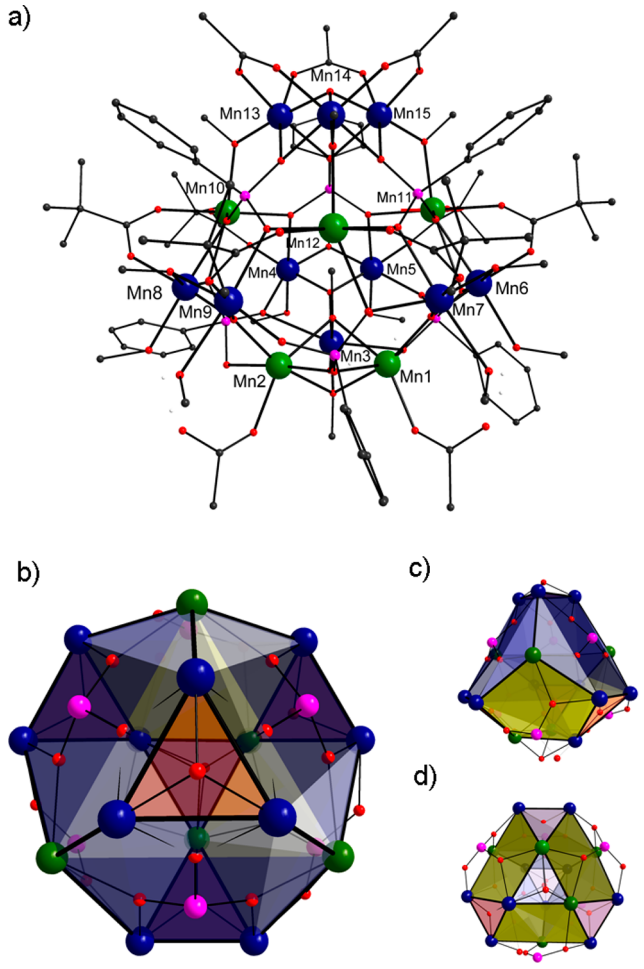


**Figure 2.** (a) Crystal structure of **2**, (b–d) core structure of the coordination cluster highlighting the topology of the molecular entity. Color scheme: $Mn^{II}$ (green), $Mn^{III}$ (blue), P (pink), C (black), O (red). H atoms omitted for clarity.

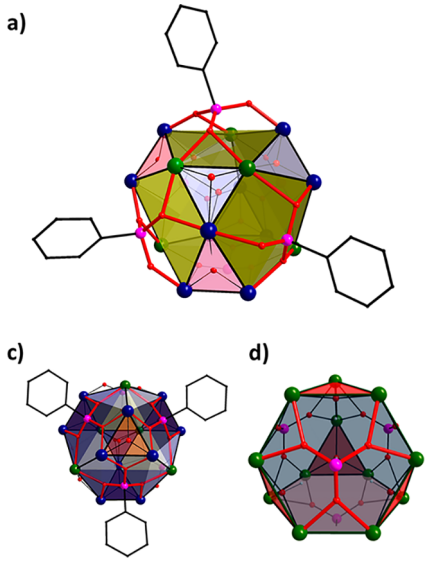


**Figure 3.** Binding modes of the organophosphonate ligands in **1** and **2**. (a) Stabilization of pentagonal faces of the core structure of **2** by phenylphosphonates. (b, c) Stabilization of hexagonal faces of the core structure of **2** and **1**, respectively. Color scheme: $Mn^{II}$ (green), $Mn^{III}$ (blue), P (pink), C (black), O (red).

The temperature dependences of the magnetic susceptibility for both, **1** and **2**, were determined between 4 and 300 K (Figure 4a). The room temperature $\chi T$ value for **1** was found

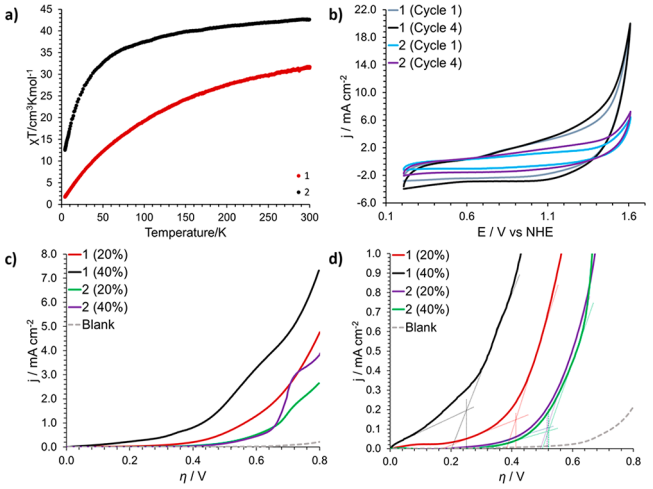


**Figure 4.** (a) Temperature dependence of magnetic susceptibility ($\chi T$) of **1** and **2**. (b) Cyclic voltammograms for **1**/**CP** and **2**/**CP** (40 wt % loading) in a KP*i* buffer solution at pH 7.2. The sudden rise in the current density with increasing potential is characteristic of catalytic water oxidation. (c) Linear sweep voltammograms for **1**/**CP** and **2**/**CP** at different loadings. (d) The determined onset potentials for **1**/**CP** and **2**/**CP** at various loadings.

to be 31.5 $cm^3$ K $mol^{-1}$ which is significantly lower than the expected value of 52.5 $cm^3$ K $mol^{-1}$ for a system of 12 independent $Mn^{II}$ ($S$ = 5/2) centers and indicative of predominantly antiferromagnetic interactions between the spin centers. This is further confirmed by the temperature-dependent behavior. When the temperature is lowered, the $\chi T$ value continuously decreases to 1.8 $cm^3$ K $mol^{-1}$ at 4 K, characteristic for an $S$ = 0 spin ground state. In the case of **2**, a $\chi T$ value of 42.6 $cm^3$ K $mol^{-1}$ was observed at room temperature which is again lower than the expected value of 51.9 $cm^3$ K $mol^{-1}$ for a system with 5 $Mn^{II}$ ($S$ = 5/2) centers and 10 $Mn^{III}$ ($S$ = 2) centers. The data demonstrates that the coupling between the Mn centers is dominantly antiferromagnetic. When the temperature is lowered to 4 K, the $\chi T$ value decreases and reaches 12.6 $cm^3$ K $mol^{-1}$. With consideration of the high $\chi T$ value at 4 K, uncompensated, competing antiferromagnetic interactions or the presence of ferromagnetic coupling between the spin centers of **2** cannot be ruled out.

A preliminary investigation of the electrochemical properties of **1** and **2** to evaluate their ability to catalyze the endergonic electron/proton-coupled $H_2O$ oxidation was conducted in aqueous medium using modified carbon paste electrodes. The latter were prepared by dispersing **1** and **2** in commercial carbon paste (**1**/**CP** and **2**/**CP**, respectively). These carbon paste based electrodes provide a hydrophobic environment and have previously been used to stabilize molecular species, preventing rapid hydrolytic decomposition even under very acidic conditions.[59] Cyclic voltammetry (CV) of both **1**/**CP** and **2**/**CP** electrodes (40 wt % loading) using a Ag/AgCl (KCl 3M) reference electrode and a Pt wire counter electrode, in potassium phosphate buffer at pH 7.2 (KP*i*, 50 mM) using $KNO_3$ (1 M) as electrolyte, results in strong catalytic waves due to $H_2O$ oxidation (Figure 4b). The similarities of the first


https://doi.org/10.1021/acs.inorgchem.1c00984
Inorg. Chem. 2021, 60, 8388–8393

and the fourth CV cycle indicate that there is no observable transformation of **1**/**CP** and **2**/**CP** during this period.

To study the kinetic profile, linear sweep voltammetry (LSV) experiments were performed using **1**/**CP** and **2**/**CP** rotating disk electrodes at a low scan rate of 1 mV/s and catalytic loadings of 20 and 40 wt % using a Ag/AgCl (KCl 3M) reference electrode and a Pt mesh counter electrode. (Figure 4c). The electrochemical profiles for both **1** and **2** clearly show that higher loadings significantly increase the current densities reaching values of 7 and 3.5 mA $cm^{-2}$, respectively (Figure 3c). The onset overpotential for **1** decreases from 413 to 251 mV with increased loadings but remains approximately constant (~520 mV) for **2** (Figure 4d and Table S6). It is noteworthy that the observed overpotential of 251 mV is among the lowest observed for polynuclear Mn compounds. Noteworthy are also the achieved current densities of **1**, particularly considering that the experiments were conducted at a pH environment close to 7. From a structural perspective, both compounds require activation prior to OER activity whereby weakly bound coordination solvent molecules can be replaced by $H_2O$ substrates. For this process, the coordination abilities of solvents and coordinating anions may be considered.[60] In **1**, this is most likely facilitated through substitution of the neutral $\mu_2$-$\kappa$O−DMSO molecules potentially resulting in a higher hydration state than the replacement of neutral terminal MeOH ligands in **2**. Considering their increased coordination ability, the negatively charged $\mu_2$-$MeO^-$ ligands in **2** may initially remain coordinated. Hence, the significantly higher activity of **1** stems from the distinctive structural differences between **1** and **2** and potentially different $O_2$ evolution mechanisms (e.g., single site vs binuclear mechanism). However, detailed future studies are required to elucidate the activity of **1**.

## CONCLUSION

To conclude, we described a synthetic approach to dodeca- and pentadecanuclear coordination clusters which represent examples of Archimedean and Johnson type solids, respectively. Both structures relate to a truncated tetrahedral geometry which is rarely observed in the chemistry of coordination clusters. The assembly approach takes advantage of sterically hindered carboxylates and strongly binding organophosphonate ligands that facilitate the formation of characteristic hexagonal structural motifs through 6.222 bridging modes of their donor atoms. Both coordination clusters are characterized by dominant antiferromagnetic exchange pathways between the spin centers. The compounds reveal distinctively different activity characteristics toward the electrocatalytic oxidation of $H_2O$. The relatively high catalytic activity of **1** in carbon paste electrodes, which is exemplified by a low onset overpotential of 251 mV and achievable current densities of 7 mA $cm^{-2}$, will be the subject of detailed future investigations.

## EXPERIMENTAL SECTION

**Synthesis of $[Mn^{II}_{12}(\mu_3-OH)_4(PhPO_3)_4(^tBuCO_2)_{12}(DMSO)_6]$·Solvent; (1·Solvent).** $Mn(MeCO_2)_2{\cdot}4H_2O$ (0.025 g, 0.10 mmol), $KMnO_4$ (0.063 g, 0.40 mmol), and pivalic acid (0.408 g, 4.00 mmol) were combined in MeCN (20 mL). After this solution was refluxed for 30 min, phenylphosphonic acid (0.032 g, 0.20 mmol) was added. Reflux was continued for ca. 10 min before L(−)-proline (0.022 g, 0.20 mmol) was added. The resultant reaction mixture was refluxed further for an additional 15 min before the light colored solution was filtered and DMSO (10 mL) was added to the filtrate. Subsequently, the solvent quantity was reduced to 1/3 of its original volume through evaporation under reduced pressure. The final reaction mixture was then filtered, and the filtrate was allowed to evaporate slowly. Pale colored crystals were obtained within 1 week. The crystals were isolated by filtration, washed with DMSO, and dried in air. Yield: ca. 20% (based on Mn).

**Synthesis of $[Mn_{15}(\mu_3-O)_4(^tBuCO_2)_{7.15}(MeCO_2)_{4.85}(PhPO_3)_6(\mu-OMe)_6(\mu_3-OMe)_2(MeOH)_5]$·Solvent (2·Solvent).** $Mn(MeCO_2)_2{\cdot}4H_2O$ (0.125 g, 0.50 mmol), $KMnO_4$ (0.016 g, 0.10 mmol), pivalic acid (0.204 g, 2.00 mmol), and glacial acetic acid (0.060 g, 1 mmol) were combined in MeCN (15 mL). After this solution was refluxed for 2 min, phenylphosphonic acid (0.040 g, 0.25 mmol) was added. The solution was then refluxed again for 2 min, and 2,6-pyridinemethanol (0.014 g, 0.10 mmol) was added. The resultant solution was refluxed again for 2 min after which MeOH (20 mL) was added to the solution, and the solution was then refluxed for 2.5 h. The dark brown/red solution was then filtered hot, and the filtrate was allowed to evaporate slowly at room temperature. Dark, rod-shaped crystals were obtained during the time period of 1 week. The crystals were isolated by filtration, washed with a MeCN/MeOH (15/20 mL) mixture, and dried in air. Yield: ca. 40% (based on Mn).

For further characterizations, see the Supporting Information.

## ASSOCIATED CONTENT

### Supporting Information

The Supporting Information is available free of charge at https://pubs.acs.org/doi/10.1021/acs.inorgchem.1c00984.

Materials and methods, experimental procedures, CHN analysis, FTIR spectra, SCXRD data, PXRD patterns, TGA analysis, and onset potential data (PDF)

### Accession Codes

CCDC 2025590−2025591 contain the supplementary crystallographic data for this paper. These data can be obtained free of charge via www.ccdc.cam.ac.uk/data_request/cif, or by emailing data_request@ccdc.cam.ac.uk, or by contacting The Cambridge Crystallographic Data Center, 12 Union Road, Cambridge CB2 1EZ, UK; fax: + 44 1223 336033.

## AUTHOR INFORMATION


### Corresponding Authors

**Graeme W. Watson** − *School of Chemistry & CRANN Institute, University of Dublin, Trinity College, Dublin 2, Ireland;* orcid.org/0000-0001-6732-9474; Email: watsong@tcd.ie

**Wolfgang Schmitt** − *School of Chemistry & CRANN Institute and AMBER Center, University of Dublin, Trinity College, Dublin 2, Ireland;* orcid.org/0000-0002-0058-9404; Email: schmittw@tcd.ie

### Authors

**Swetanshu Tandon** − *School of Chemistry & CRANN Institute and AMBER Center, University of Dublin, Trinity College, Dublin 2, Ireland;* orcid.org/0000-0002-0626-0626

**Friedrich W. Steuber** − *School of Chemistry & CRANN Institute and AMBER Center, University of Dublin, Trinity College, Dublin 2, Ireland*

**Amal C. Kathalikkattil** − *School of Chemistry & CRANN Institute and AMBER Center, University of Dublin, Trinity College, Dublin 2, Ireland;* orcid.org/0000-0002-7351-0357

**Munuswamy Venkatesan** − *School of Physics & CRANN Institute, University of Dublin, Trinity College, Dublin 2, Ireland*




https://doi.org/10.1021/acs.inorgchem.1c00984
Inorg. Chem. 2021, 60, 8388−8393

Complete contact information is available at:
https://pubs.acs.org/10.1021/acs.inorgchem.1c00984

### Notes

The authors declare no competing financial interest.

## ■ ACKNOWLEDGMENTS

The authors would like to thank Dr. Brendan Twamley for his help with the crystallographic characterization of the compounds. This work was supported by the Irish Research Council (GOIPG/2015/2952), Science Foundation Ireland (13/IA/1896) and the European Research Council (CoG 2014−647719).

## ■ REFERENCES

(1) Aromí, G.; Brechin, E. K. In *Single-Molecule Magnets and Related Phenomena*; Winpenny, R., Ed.; Springer Berlin Heidelberg: Berlin, Heidelberg, 2006; pp 1−67.
(2) Gatteschi, D.; Sessoli, R.; Villain, J. *Molecular Nanomagnets*. Oxford University Press: Oxford, 2006; p 1−395.
(3) Northrop, B. H.; Zheng, Y.-R.; Chi, K.-W.; Stang, P. J. Self-Organization in Coordination-Driven Self-Assembly. *Acc. Chem. Res.* **2009**, *42* (10), 1554−1563.
(4) Beltran, L. M. C.; Long, J. R. Directed Assembly of Metal−Cyanide Cluster Magnets. *Acc. Chem. Res.* **2005**, *38* (4), 325−334.
(5) Kortz, U.; Müller, A.; van Slageren, J.; Schnack, J.; Dalal, N. S.; Dressel, M. Polyoxometalates: Fascinating structures, unique magnetic properties. *Coord. Chem. Rev.* **2009**, *253* (19), 2315−2327.
(6) Kostakis, G. E.; Ako, A. M.; Powell, A. K. Structural motifs and topological representation of Mn coordination clusters. *Chem. Soc. Rev.* **2010**, *39* (6), 2238−2271.
(7) He, Y.-P.; Yuan, L.-B.; Chen, G.-H.; Lin, Q.-P.; Wang, F.; Zhang, L.; Zhang, J. Water-Soluble and Ultrastable $Ti_4L_6$ Tetrahedron with Coordination Assembly Function. *J. Am. Chem. Soc.* **2017**, *139* (46), 16845−16851.
(8) He, Y.-P.; Chen, G.-H.; Yuan, L.-B.; Zhang, L.; Zhang, J. $Ti_4$(embonate)$_6$ Cage-Ligand Strategy on the Construction of Metal−Organic Frameworks with High Stability and Gas Sorption Properties. *Inorg. Chem.* **2020**, *59* (2), 964−967.
(9) Caneschi, A.; Gatteschi, D.; Sessoli, R. Manganese clusters: a common ground for photosynthesis, quantum tunnelling of the magnetization and colossal magnetoresistance. *J. Chem. Soc., Dalton Trans.* **1997**, No. 21, 3963−3970.
(10) Jones, L. F.; Brechin, E. K.; Collison, D.; Harrison, A.; Teat, S. J.; Wernsdorfer, W. New routes to high nuclearity cages: a fluoride-based hexaicosametallic manganese cage. *Chem. Commun.* **2002**, No. 24, 2974−2975.
(11) Tasiopoulos, A. J.; Vinslava, A.; Wernsdorfer, W.; Abboud, K. A.; Christou, G. Giant Single-Molecule Magnets: A $\{Mn_{84}\}$ Torus and Its Supramolecular Nanotubes. *Angew. Chem., Int. Ed.* **2004**, *43* (16), 2117−2121.
(12) Ako, A. M.; Hewitt, I. J.; Mereacre, V.; Clérac, R.; Wernsdorfer, W.; Anson, C. E.; Powell, A. K. A Ferromagnetically Coupled $Mn_{19}$ Aggregate with a Record S = 83/2 Ground Spin State. *Angew. Chem., Int. Ed.* **2006**, *45* (30), 4926−4929.
(13) Manoli, M.; Inglis, R.; Manos, M. J.; Nastopoulos, V.; Wernsdorfer, W.; Brechin, E. K.; Tasiopoulos, A. J. A $[Mn_{32}]$ Double-Decker Wheel. *Angew. Chem., Int. Ed.* **2011**, *50* (19), 4441−4444.
(14) Manoli, M.; Inglis, R.; Manos, M. J.; Papaefstathiou, G. S.; Brechin, E. K.; Tasiopoulos, A. J. A 1-D coordination polymer based on a $Mn_{40}$ octagonal super-structure. *Chem. Commun.* **2013**, *49* (11), 1061−1063.
(15) Alexandropoulos, D. I.; Fournet, A.; Cunha-Silva, L.; Christou, G.; Stamatatos, T. C. Molecular Nanoclusters": A 2-nm-Sized $\{Mn_{29}\}$ Cluster with a Spherical Structure. *Inorg. Chem.* **2016**, *55* (23), 12118−12121.
(16) Manoli, M.; Alexandrou, S.; Pham, L.; Lorusso, G.; Wernsdorfer, W.; Evangelisti, M.; Christou, G.; Tasiopoulos, A. J. Magnetic "Molecular Oligomers" Based on Decametallic Supertetrahedra: A Giant $Mn_{49}$ Cuboctahedron and its $Mn_{25}Na_4$ Fragment. *Angew. Chem., Int. Ed.* **2016**, *55* (2), 679−684.
(17) Zheng, Y.-Z.; Zhou, G.-J.; Zheng, Z.; Winpenny, R. E. P. Molecule-based magnetic coolers. *Chem. Soc. Rev.* **2014**, *43* (5), 1462−1475.
(18) Manoli, M.; Collins, A.; Parsons, S.; Candini, A.; Evangelisti, M.; Brechin, E. K. Mixed-Valent Mn Supertetrahedra and Planar Discs as Enhanced Magnetic Coolers. *J. Am. Chem. Soc.* **2008**, *130* (33), 11129−11139.
(19) Charalambous, M.; Moushi, E. E.; Nguyen, T. N.; Papatriantafyllopoulou, C.; Nastopoulos, V.; Christou, G.; Tasiopoulos, A. J. Giant Heterometallic $[Mn_{36}Ni_4]^{0/2-}$ and $[Mn_{32}Co_8]$ "Loops-of-Loops-and-Supertetrahedra" Molecular Aggregates. *Frontiers in Chemistry* 2019, *7* (96).
(20) Kessissoglou, D. P. In *Bioinorganic Chemistry: An Inorganic Perspective of Life*; Kessissoglou, D. P., Ed.; Springer: Netherlands: Dordrecht, 1995; pp 299−320.
(21) McEvoy, J. P.; Brudvig, G. W. Water-splitting chemistry of photosystem II. *Chem. Rev.* **2006**, *106* (11), 4455−4483.
(22) Dau, H.; Zaharieva, I. Principles, Efficiency, and Blueprint Character of Solar-Energy Conversion in Photosynthetic Water Oxidation. *Acc. Chem. Res.* **2009**, *42* (12), 1861−1870.
(23) Miller, A.-F. Superoxide dismutases: Ancient enzymes and new insights. *FEBS Lett.* **2012**, *586* (5), 585−595.
(24) Krishnan, K. K.; Thomas, A. M.; Sindhu, K. S.; Anilkumar, G. Recent advances and perspectives in the manganese-catalysed epoxidation reactions. *Tetrahedron* **2016**, *72* (1), 1−16.
(25) Perez-Navarro, M.; Neese, F.; Lubitz, W.; Pantazis, D. A.; Cox, N. Recent developments in biological water oxidation. *Curr. Opin. Chem. Biol.* **2016**, *31*, 113−119.
(26) Valyaev, D. A.; Lavigne, G.; Lugan, N. Manganese organometallic compounds in homogeneous catalysis: Past, present, and prospects. *Coord. Chem. Rev.* **2016**, *308*, 191−235.
(27) Cano, R.; Mackey, K.; McGlacken, G. P. Recent advances in manganese-catalysed C-H activation: scope and mechanism. *Catal. Sci. Technol.* **2018**, *8* (5), 1251−1266.
(28) Grills, D. C.; Ertem, M. Z.; McKinnon, M.; Ngo, K. T.; Rochford, J. Mechanistic aspects of $CO_2$ reduction catalysis with manganese-based molecular catalysts. *Coord. Chem. Rev.* **2018**, *374*, 173−217.
(29) Al-Oweini, R.; Sartorel, A.; Bassil, B. S.; Natali, M.; Berardi, S.; Scandola, F.; Kortz, U.; Bonchio, M. Photocatalytic Water Oxidation by a Mixed-Valent $Mn^{III}_3Mn^{IV}O_3$ Manganese Oxo Core that Mimics the Natural Oxygen-Evolving Center. *Angew. Chem., Int. Ed.* **2014**, *53* (42), 11182−11185.
(30) Schwarz, B.; Forster, J.; Goetz, M. K.; Yucel, D.; Berger, C.; Jacob, T.; Streb, C. Visible-Light-Driven Water Oxidation by a Molecular Manganese Vanadium Oxide Cluster. *Angew. Chem., Int. Ed.* **2016**, *55* (21), 6329−6333.
(31) Maayan, G.; Gluz, N.; Christou, G. A bioinspired soluble manganese cluster as a water oxidation electrocatalyst with low overpotential. *Nat. Catal.* **2018**, *1* (1), 48−54.
(32) Ghosh, T.; Maayan, G. Efficient Homogeneous Electrocatalytic Water Oxidation by a Manganese Cluster with an Overpotential of Only 74 mV. *Angew. Chem., Int. Ed.* **2019**, *58* (9), 2785−2790.
(33) Gao, Y. L.; Crabtree, R. H.; Brudvig, G. W. Water Oxidation Catalyzed by the Tetranuclear Mn Complex $[Mn^{IV}_4O_5$(terpy)$_4(H_2O)_2](ClO_4)_6$. *Inorg. Chem.* **2012**, *51* (7), 4043−4050.
(34) Tandon, S.; Soriano-López, J.; Kathalikkattil, A. C.; Jin, G.; Wix, P.; Venkatesan, M.; Lundy, R.; Morris, M. A.; Watson, G. W.; Schmitt, W. A cubane-type manganese complex with $H_2O$ oxidation capabilities. *Sustain. Energy Fuels* **2020**, *4* (9), 4464−4468.
(35) Soriano-López, J.; Elliott, R.; Kathalikkattil, A. C.; Ako, A. M.; Mulahmetović, M.; Venkatesan, M.; Schmitt, W. Bioinspired Water Oxidation Using a Mn-Oxo Cluster Stabilized by Non-Innocent

Organic Tyrosine Y161 and Plastoquinone Mimics. *ACS Sustainable Chem. Eng.* **2020**, *8* (36), 13648−13659.
(36) Bard, A. J.; Fox, M. A. Artificial Photosynthesis - Solar Splitting of Water to Hydrogen and Oxygen. *Acc. Chem. Res.* **1995**, *28* (3), 141−145.
(37) Yano, J.; Yachandra, V. $Mn_4Ca$ Cluster in Photosynthesis: Where and How Water is Oxidized to Dioxygen. *Chem. Rev.* **2014**, *114* (8), 4175−4205.
(38) Winpenny, R. E. P. Serendipitous assembly of polynuclear cage compounds. *J. Chem. Soc., Dalton Trans.* **2002**, No. 1, 1−10.
(39) Holden, A. *Shapes, Space, and Symmetry*. Dover Publications: 1991.
(40) Zhang, L.; Schmitt, W. From Platonic Templates to Archimedean Solids: Successive Construction of Nanoscopic $\{V_{16}As_8\}$, $\{V_{16}As_{10}\}$, $\{V_{20}As_8\}$, and $\{V_{24}As_8\}$ Polyoxovanadate Cages. *J. Am. Chem. Soc.* **2011**, *133* (29), 11240−11248.
(41) Zhang, L.; Clérac, R.; Heijboer, P.; Schmitt, W. Influencing the Symmetry of High-Nuclearity and High-Spin Manganese Oxo Clusters: Supramolecular Approaches to Manganese-Based Keplerates and Chiral Solids. *Angew. Chem., Int. Ed.* **2012**, *51* (12), 3007−3011.
(42) Zhang, L.; Chimamkpam, T.; Onet, C. I.; Zhu, N.; Clérac, R.; Schmitt, W. Anion-directed supramolecular chemistry modulating the magnetic properties of nanoscopic Mn coordination clusters: from polynuclear high-spin complexes to SMMs. *Dalton Trans.* **2016**, *45* (44), 17705−17713.
(43) Johnson, N. W. Convex Polyhedra with Regular Faces. *Can. J. Math.* **1966**, *18*, 169−200.
(44) Poyraz, M.; Sari, M.; Cevik, S.; Buyukgungor, O. Redetermination of the mixed-valence hexa-nuclear manganese oxide complex di-mu(4)-oxo-tetra-mu(3)-pivalato-hexa-mu(2)-pivalato-tetrakis-(pivalic acid)dimanganese(III)tetra-manganese(II) at 100 K. *Acta Crystallogr., Sect. E: Struct. Rep. Online* **2006**, *62*, M1442−M1444.
(45) Astakhov, G. S.; Bilyachenko, A. N.; Korlyukov, A. A.; Levitsky, M. M.; Shul'pina, L. S.; Bantreil, X.; Lamaty, F.; Vologzhanina, A. V.; Shubina, E. S.; Dorovatovskii, P. V.; Nesterov, D. S.; Pombeiro, A. J. L.; Shul'pin, G. B. High-Cluster ($Cu_9$) Cage Silsesquioxanes: Synthesis, Structure, and Catalytic Activity. *Inorg. Chem.* **2018**, *57* (18), 11524−11529.
(46) Astakhov, G. S.; Bilyachenko, A. N.; Levitsky, M. M.; Korlyukov, A. A.; Zubavichus, Y. V.; Dorovatovskii, P. V.; Khrustalev, V. N.; Vologzhanina, A. V.; Shubina, E. S. Tridecanuclear $Cu^{II}_{11}Na_2$ Cagelike Silsesquioxanes. *Cryst. Growth Des.* **2018**, *18* (9), 5377−5384.
(47) Bilyachenko, A. N.; Levitsky, M. M.; Korlyukov, A. A.; Khrustalev, V. N.; Zubavichus, Y. V.; Shul'pina, L. S.; Shubina, E. S.; Vologzhanina, A. V.; Shul'pin, G. B. Heptanuclear Cage $Cu^{II}$-Silsesquioxanes: Synthesis, Structure and Catalytic Activity. *Eur. J. Inorg. Chem.* **2018**, *2018* (22), 2505−2511.
(48) Keggin, J. F. Structure of the Molecule of 12-Phosphotungstic Acid. *Nature* **1933**, *131* (3321), 908−909.
(49) Coxall, R. A.; Harris, S. G.; Henderson, D. K.; Parsons, S.; Tasker, P. A.; Winpenny, R. E. P. Inter-ligand reactions: in situ formation of new polydentate ligands. *J. Chem. Soc., Dalton Trans.* **2000**, No. 14, 2349−2356.
(50) Brown, I. D.; Altermatt, D. Bond-valence parameters obtained from a systematic analysis of the Inorganic Crystal Structure Database. *Acta Crystallogr., Sect. B: Struct. Sci.* **1985**, *41* (4), 244−247.
(51) Brown, I. D. Recent Developments in the Methods and Applications of the Bond Valence Model. *Chem. Rev.* **2009**, *109* (12), 6858−6919.
(52) van Slageren, J.; Rosa, P.; Caneschi, A.; Sessoli, R.; Casellas, H.; Rakitin, Y. V.; Cianchi, L.; Giallo, F. D.; Spina, G.; Bino, A.; Barra, A.-L.; Guidi, T.; Carretta, S.; Caciuffo, R. Static and dynamic magnetic properties of an $[Fe_{13}]$ cluster. *Phys. Rev. B: Condens. Matter Mater. Phys.* **2006**, *73* (1), 014422.
(53) Breeze, B. A.; Shanmugam, M.; Tuna, F.; Winpenny, R. E. P. A series of nickel phosphonate−carboxylate cages. *Chem. Commun.* **2007**, No. 48, 5185−5187.
(54) Sheikh, J. A.; Adhikary, A.; Jena, H. S.; Biswas, S.; Konar, S. High Nuclearity (Octa-, Dodeca-, and Pentadecanuclear) Metal (M = $Co^{II}$, $Ni^{II}$) Phosphonate Cages: Synthesis, Structure, and Magnetic Behavior. *Inorg. Chem.* **2014**, *53* (3), 1606−1613.
(55) Frost, J. M.; Sanz, S.; Rajeshkumar, T.; Pitak, M. B.; Coles, S. J.; Rajaraman, G.; Wernsdorfer, W.; Schnack, J.; Lusby, P. J.; Brechin, E. K. A truncated $[Mn^{III}_{12}]$ tetrahedron from oxime-based $[Mn^{III}_3O]$ building blocks. *Dalton Trans.* **2014**, *43* (28), 10690−10694.
(56) Pinsky, M.; Avnir, D. Continuous symmetry measures. 5. The classical polyhedra. *Inorg. Chem.* **1998**, *37* (21), 5575−5582.
(57) Cirera, J.; Ruiz, E.; Alvarez, S. Continuous Shape Measures as a Stereochemical Tool in Organometallic Chemistry. *Organometallics* **2005**, *24* (7), 1556−1562.
(58) Llunell, M.; Casanova, D.; Cirera, J.; Alemany, P.; Alvarez, S. *SHAPE Version 2.1* **2013**.
(59) Blasco-Ahicart, M.; Soriano-López, J.; Carbó, J. J.; Poblet, J. M.; Galan-Mascaros, J. R. Polyoxometalate electrocatalysts based on earth-abundant metals for efficient water oxidation in acidic media. *Nat. Chem.* **2018**, *10* (1), 24−30.
(60) Alvarez, S. Coordinating Ability of Anions, Solvents, Amino Acids, and Gases towards Alkaline and Alkaline-Earth Elements, Transition Metals, and Lanthanides. *Chem. - Eur. J.* **2020**, *26* (19), 4350−4377.


https://doi.org/10.1021/acs.inorgchem.1c00984
*Inorg. Chem.* 2021, 60, 8388−8393